Momentum and Boltzmann distributions of neon fragments at ~300 MeV/nucleon

M. M. Aggarwal and P. L. Jain
High Energy Experimental Laboratory, Department of Physics, State University of New York at Buffalo, Buffalo, New York 14260
(Received 7 September 1984)

The interaction cross section of a neon beam at ~300 MeV/nucleon along with the partial production cross sections of its fragments is studied in nuclear emulsion. Projected angular distributions of fragments are measured and are correlated with the longitudinal momentum distributions which enable us to estimate the Fermi momentum of the projectile. The space angle distributions of singly and doubly charged particles are discussed on the basis of the Boltzmann distributions.

I. INTRODUCTION

Much interest has been shown both experimentally and theoretically in the study of heavy-ion collisions because of the availability of the nuclear beams at the Berkeley Bevalac. For heavy-ion reactions well above the Coulomb barrier, emission of α particles corresponds to a large fraction of the total reaction cross section. Recently[1] we studied the angular distributions of relativistic α particles produced from Fe-emulsion and Ar-emulsion interactions at energies ≥ 1 GeV/nucleon and observed two separate classes of alphas with different characteristics. They seem to come from two different sources with different production mechanisms.

In this paper we present the results on the Ne-emulsion interactions at ~300 MeV/nucleon. Section III A deals with the general characteristics of interactions, such as production cross sections of the fragments, two product fragmentations, and multiplicities of different kinds of particles. In Sec. III C an attempt has been made to estimate the spread in the longitudinal momenta of the fragments which are produced in the projectile and target fragmentation events. These momenta have been determined from the projected angles of the fragments and have enabled us to estimate the Fermi momentum. Section III C deals with the production of singly and doubly charged fragments produced in Ne-emulsion collisions. The angular distributions of singly and doubly charged fragments have been compared with the moving Boltzmann distributions. In order to explain the fragmentation peak and tail simultaneously, it is assumed that a thermal source such as a fireball, formed from the nucleons mutually swept out from the target and projectile, is produced which accounts for the tail part of the distribution. The different parameters of the fireball, viz., the velocity (β) and temperature (T), are calculated assuming the isotropic decay in the rest frame of the fireball. The characteristics of the tail distributions are discussed with respect to the different types of events.

II. EXPERIMENTAL DETAILS

A stack of Ilford G-5 emulsion pellicles of 600 μm thickness and of dimensions 10×8 cm^2 was exposed to a 300 MeV/nucleon, ^{20}Ne beam at the Berkeley Bevalac. The beam was parallel to the emulsion plane with a flux density of 10^3 particles/cm^2. An along-the-track scanning technique was used to locate events under 45 x air objective. We thus collected 851 events. Each interaction was scrutinized under 100 x oil immersion objective to count and classify the different types of tracks. The tracks produced in an interaction are generally classified into three types on the basis of their grain density (g) measurements, viz., (i) singly charged tracks n_p, those with $g \leq 1.5g_p$; and (ii) the grey tracks (N_g) for which $1.5g_p < g \leq 4.5g_p$ and black tracks (N_b) with $g > 4.5g_p^2$. Here g_p corresponds to the grain density of a minimum ionizing track. The total number of black and grey tracks is denoted by N_h (i.e., $N_h = N_b + N_g$). The interactions were quantitatively classified as: (i) pure projectile fragmentation (P), with no visible target fragment, known as white stars, with $N_h = 0$ (N_h is the number of nonrelativistic tracks); (ii) target fragmentation (T) only with no detectable change in the charge of the projectile; (iii) projectile breakup with target fragmentation $N_h \geq 1$ ($P+T$); and (iv) central events with no forward cone fragments from the projectile. The percentages for different categories are (13 ± 1), (4 ± 1), (72 ± 3), and (10 ± 1), respectively. The events with $1 \leq N_h \leq 6$ are $(53\pm 3)\%$ and the events with $N_h > 6$ are $(35\pm 2)\%$, which are about the same as found in proton-emulsion nuclei interactions. The charges of the projectile fragments were determined from charge conservation and were checked with δ-ray and gap density measurements.[2] In order to calculate the space and projected angles of the tracks with respect to the beam direction, we measured, on each beam and the track under consideration, x, y, and z coordinates separated by at least 500 μm from the interaction vertex in the forward cone.

III. RESULTS AND DISCUSSION

A. Total and partial production cross sections

We followed about 105 m of track length of a primary neon beam in nuclear emulsion and obtained 851 interactions. The mean free path is 12.4 ± 0.4 cm which corresponds to cross section $(\sigma_{0b}) = (1021\pm 35)$ mb. We have made the calculations for the interaction cross section from the geometrical formula first proposed by Bradt and Peters[3] which is given as

TABLE I. Comparison of the experimentally observed cross section in emulsion with the theoretically calculated ones for C, Ne, Si, Ar, Fe, Kr, and U.

Projectile	Cross section in mb		
	Experiment	Theory Eq. (1)[a]	Eq. (2)[b]
Carbon	850±28	965	824
Neon	1021±35	1164	1036
Silicon	1161±38	1328	1209
Argon	1406±48	1540	1429
Iron	1583±53	1783	1679
Krypton	1898±42	2144	2049
Uranium	3449±115	3580	3508

[a] $r_0=1.36$, $b=0.83$.
[b] $r_0=1.36$, $b_0=1.3$.

$$\sigma_{BT}=\pi r_0^2(A_B^{1/3}+A_T^{1/3}-b)^2\,, \tag{1}$$

where A_B and A_T are the mass numbers of the beam and target, respectively; b is the overlap parameter, and r_0 is the constant of proportionality in the expression for the geometrical nuclear radius, i.e., $r_i=r_0A_i^{1/3}$. In order to calculate σ_{BT} for neon-emulsion interactions, we used the composition of emulsion as given by Barkas.[4] σ_{BT} for different elements of emulsion were determined using Eq. (1) for $r_0=1.36$ and $b=0.83$.[5] The proper averaging over the different elements of emulsion yielded $\sigma_{BT}=1164$ mb for neon-emulsion interactions. This value is large as compared to the observed value of σ_{BT} (i.e., 1021±35 mb). Barshay *et al.*[6] found that Glauber amplitudes in nucleus-nucleus scattering also lead to a nucleus-nucleus interaction cross section which can be expressed in the above-mentioned form,

$$\sigma_{BT}=\pi r_0^2[A_B^{1/3}+A_T^{1/3}-b_0(A_B^{-1/3}+A_T^{-1/3})]^2\ \text{fm}^2\,, \tag{2}$$

where $r_0=1.36$ fm and $b_0=0.75$. We find that $b_0=1.3$ gives reasonably good agreement with the emulsion data, as shown in Table I. σ_{BT} calculated using Eq. (2) for $r_0=1.36$ fm and $b_0=1.3$ is 1036 mb. This is close to the experimental observed value. Comparison of experimental observations with Eq. (2) for other beams used in our laboratory is quite good, as shown in Table I.

TABLE II. Partial production cross sections of different kinds of fragments produced by a Ne beam in its interaction with emulsion.

Fragment type	Cross section in mb at two energies	
	≤165 MeV/nucleon	(165–300) MeV/nucleon
He	560±40	730±50
Li	120±20	82±20
Be	73±20	67±20
B	31±10	77±20
C	90±20	90±20
N	90±20	90±20
O	136±20	117±20
F	60±10	18±10

In Table II the partial production cross sections for different kinds of projectile fragments for $E\leq 165$ MeV/nucleon and $165<E\leq 300$ MeV/nucleon are shown. It is seen that the production cross section for O, N, C, B, and Be are identical within the statistical errors at both the energies. Kullberg *et al.*[7] also did not notice any difference in production cross sections of N, C, B, and Be fragments produced in O-emulsion interactions at 0.2 and 2.1 GeV/nucleon energies. In the present study, the production cross section for Li fragments is greater at low energy (i.e., <165 MeV/nucleon) than that at high energy (i.e., >165 MeV/nucleon), in agreement with Ref. 7, whereas for the He fragments it is greater at high energy than that at low energy and it disagrees with that of Kullberg *et al.*[7] The production cross section for the emission of one to five He fragments is listed in Table III. It is seen that the cross section decreases systematically with an increase in the number of He fragments. This result disagrees with published work[7,8] which has basically reported the constancy in the production of one to three He fragments. Overall, the cross section of the He fragments agrees with that of He fragments produced in O-emulsion nuclei[9] interactions at high energy. The average numbers of heavy prongs, N_h, for interactions with one to five He fragments are also listed in Table III. It is obvious that $\langle N_h\rangle$ is constant for interactions with one, two, or three He fragments, whereas for four He fragments it is less. We just observed two events with five He fragments both with $N_h=0$. This result seems to be in agreement with that of Ref. 7 and quite in disagreement with that of Jakobsson and Kullberg,[8] who found that $\langle N_h\rangle$ decreases with increasing He multiplicity at 2 GeV/nucleon. This difference may be due to the increase in the incident energy, and needs further investigation.

Table IV lists the frequency of interactions with the emission of Li from the projectile along with other multiply charged fragments. We also included in this table the data at different energies from other laboratories. Our percentages are in good agreement with that of O-emulsion interactions at 0.2 GeV/nucleon. We observe that about 70% of the Li fragments are produced along with the emission of at least one more Li or together with one or more He fragments, whereas in an oxygen beam at the same energy its production rate is 90%, and at higher energy it is only ~50%. We also find that about 65% of the O fragments in the present work are emitted along with the He fragment. Thus it seems that modes of fragmentation are almost the same for ^{20}Ne and ^{16}O nuclei except for small differences which are primarily due to the differences in their masses.

It is worth mentioning that at low energy we observe 22 events of neon fragmentation which have two or more projectile fragments with $Z>2$, such as Ne→Be + Be or Be + B, etc. Thus the cross section for two product fragmentation is (36±8) mb at 300 MeV/nucleon. At higher energy, i.e., at 2.1 GeV/nucleon, Heckman *et al.*[10] did not observe a single such event for ^{12}C, ^{14}N, and ^{16}O projectiles out of 1000 observed interactions for each projectile. Thus we see that the two-product fragmentation cross section is highly suppressed with an increase in the incident energy.

TABLE III. σ(mb) and $\langle N_h \rangle$ in interactions with different numbers of He fragments.

No. of He fragments	Ne-emulsion at 0.3 GeV/nucleon Present work		σ (mb) and $\langle N_h \rangle$ O-emulsion at 0.2 GeV[7]/nucleon		O-emulsion at 2 GeV[8]/nucleon	
	σ (mb)	$\langle N_h \rangle$	σ (mb)	$\langle N_h \rangle$	σ (mb)	$\langle N_h \rangle$
1	340±22	5.9±0.4	250±30	4.2±0.3	190±30	11.2±0.8
2	150±15	5.3±0.5	320±40	3.7±0.3	190±40	7.2±1.4
3	80±11	5.5±0.8	220±30	2.5±0.4	270±40	3.3±0.5
4	30±6	3.7±0.8	40±10	0.7±0.2	10	
5	3±2					

B. Dependence of $\langle N_h \rangle$, $\langle n_p \rangle$, and $\langle n_\alpha \rangle$ on Z_{max}

The percentages of events with Z_{max} (the highest charged fragment in an event) $=1$, 2, 3, and ≥ 4 are (10±1), (29±2), (10±1), and (51±3), respectively. Percentages of events for different values of Z_{max} can be compared with those of O-emulsion interactions at 2.1 GeV/nucleon.[10] Percentages of events for $Z_{max}=1$, 2, 3, and ≥ 4 are (2±1), (33±5), (9±2), and (55±1), respectively. There is much discrepancy for events with $Z_{max}=1$ and it seems that by increasing the incident energy the percentage of such events decreases, whereas Kullberg *et al.*[7] reported that this percentage increases with increasing incident energy. Our results for $Z_{max} \geq 2$ seem to be in agreement with those of O-emulsion nuclei interactions at 2.1 GeV/nucleon. As mentioned earlier, there seems to be a similarity in the production cross sections for different projectiles.

Figure 1 shows the variations of $\langle n_p \rangle$, $\langle n_\alpha \rangle$, and $\langle N_h \rangle$ as a function of Z_{max}. It is seen that $\langle n_p \rangle$ for $Z_{max}=1$ is only (5.6±0.7) and it is about four units of charges less than the charge of the projectile. For such events $\langle N_h \rangle$ is (16.9±2.1), which seems to be quite large as compared to that for ^{16}O, which is (10.0±0.5).[7] It seems at this low energy some protons might have been taken as heavy tracks. Thus, the decrease of $\langle n_p \rangle$ for such events may partly be because some of the low energy tracks might have been taken as grey tracks and partly due to the undetected singly charged particles. Also, it can be accounted for by charge exchange reactions between the projectile and target nucleon, i.e., $p \rightarrow n$. For $Z_{max} > 1$, the total charge of the fragments is approximately equal to the charge of the projectile. Thus we do not see any excess of charge in the total charge of the fragments over the charge of the projectile. It seems that the pion production at this low energy of 300 MeV/nucleon is negligible. For further analysis it is assumed that all the singly charged particles are baryons. It is seen from the figure that $\langle n_p \rangle$ decreases in steps with an increase in Z_{max}, and the same is true for $\langle n_\alpha \rangle$. $\langle N_h \rangle$ seems to stay constant for $Z_{max} \geq 6$ and it is quite a bit less. Such events seem to represent the peripheral-type collisions, i.e., the collisions with a large impact parameter. For $Z_{max} < 6$ $\langle N_h \rangle$ is a decreasing function of Z_{max}, which indicates that these events correspond to different values of the impact parameter for $Z_{max}=1$ representing the central collision. $\langle N_h \rangle$ represents the degree of target excitation, which to some extent is dependent on the impact parameter of the collision. Thus, we see that the impact parameter seems to increase with increasing Z_{max} up to $Z_{max}=5$ and then it stays almost constant. It is interesting to note that $\langle N_h \rangle$ is larger when $\langle n_p \rangle$ and $\langle n_\alpha \rangle$ are larger, which means that $\langle N_h \rangle$ increases as the degree of breakup of the projectile increases.

C. Momentum distributions

Experimental studies of fragmentation of heavy-ion nuclei on various targets have revealed that when a projectile nucleus breaks up in its interaction with the target, it fragments into nuclei with the momenta narrowly distributed about the momentum of the projectile. The spread in the momentum is found to be of the order of the "Fermi momentum" of the projectile. This can be determined from the angular widths of the projected angular distribution for a particular fragment. The projected angular distributions are found to be compatible with the Gaussian distribution. The standard deviation $[\sigma(p)]$ of the momentum distributions of the emitted fragments is related to the observed angular widths $\sigma(\theta)$ as

$$\sigma(p) = p_B A_f \sin[\sigma(\theta)] , \tag{3}$$

TABLE IV. Percentages of interactions with emission of Li from the projectile nucleus along with other fragments.

Beam	Energy (GeV/nucleon)	Fragmentation channel Li + N	Li + He + N	Li + 2*He + N	2*Li + N	2*Li + He	Reference
Ne	0.3	2.9±0.6	3.8±0.7	2.1±0.6	0.6±0.3	0.7±0.4	This work
O	0.2	1.6±0.6	4.5±1.0	2.9±0.8	1.8±0.6	0.8±0.4	7
O	2.1	3.3±0.8	1.2±0.5	0.5±0.3			8
O	2.0	2.0±0.8	3.0±1.0	0.7±0.5			9

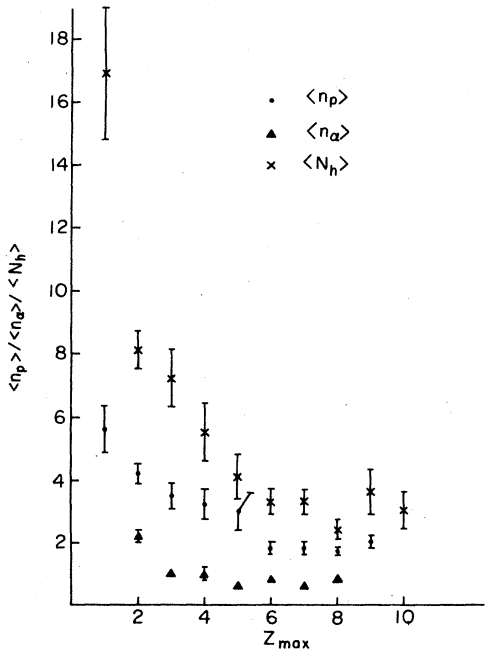

FIG. 1. The variations of $\langle N_h \rangle$, $\langle n_p \rangle$, and $\langle N_\alpha \rangle$ vs Z_{max} (the highest charged projectile fragment produced in an event).

where p_B is the beam momentum per nucleon and A_f is the mass number of the fragment.

Figure 2(a) shows the projected angular distribution of the singly charged particles for events with $N_h=0$, i.e., pure projectile fragmentation events with no detectable target excitation. These events are regarded as representing the nuclear collision at a large impact parameter. This distribution peaks around 1° with a large angular width and has a long tail. We fitted double Gaussian distributions of the form

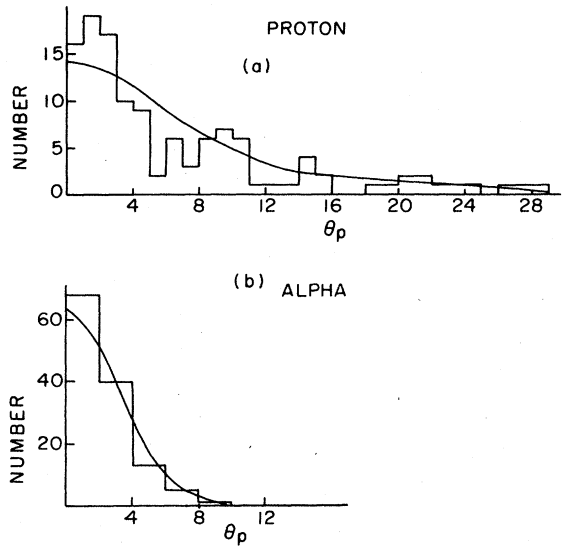

FIG. 2. The projected angular distributions (a) for $Z=1$ fragments and (b) for $Z=2$ fragments produced in $N_h=0$ events. The curves correspond to a fit due to Eq. (4).

TABLE V. Standard deviation widths of the momentum distributions $\sigma(p)$ for the singly and doubly charged particles produced in $N_h=0$ events.

Fragment (weight)	Experiment: Present work (MeV/c)	Experiment: (Ref. 12) for CNO	Calculated (Ref. 11) Eq. (5) (MeV/c)
$Z=1$	63±7		
p (0.74)		69±6	77
d (0.19)		134±4	106
t (0.07)		144±6	126
$Z=2$	140±15		
^{3}He (0.24)		150±6	126
^{4}He (0.76)		130±1	141

$$N(\theta)=A\exp[-\theta^2/2\sigma_1^2]+B\exp[-\theta^2/2\sigma_2^2] \quad (4)$$

and obtained $\sigma_1=5.59°$ and $\sigma_2=13.86°$ as the standard deviations for the peak and tail, respectively. $\sigma(p)$ computed from Eq. (3) is listed in Table V. Table V also includes the expected values of $\sigma(p)$ calculated using the formula given by Lepore and Riddell.[11] Following these authors the standard deviation of the projected momentum distribution, which is a Gaussian distribution, can be written as

$$\sigma(p)=[m_n(45A_B^{-1/3}-25A_B^{-2/3})A_f(A_B-A_f)/2A_B]^{1/2}\,. \quad (5)$$

It is seen that the observed $\sigma(p)$ is close to that of the proton fragment and is very low compared to that of singly charged particles. Table V also lists the experimental values obtained by Greiner *et al.*,[12] which are close to those calculated using the Lepore and Riddell[11] theory. We see that tail distribution is also described by a Gaussian distribution with an amplitude of about one-third that of the peak. We mentioned in Sec. III B that pion production at this energy can be approximately neglected. Thus the large angle singly charged particles are primarily protons. The width of the momentum distribution corresponding to $\sigma_2=13.85$ is 154 MeV/c. This value may be

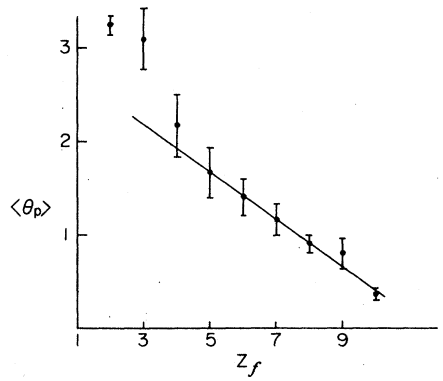

FIG. 3. The plot of $\langle \theta_p \rangle$ vs Z_f. Here, θ_p is the projected angle of the fragment with respect to the beam and Z_f is the charge of the fragment. The solid line drawn through the data is to guide the eye.

compared with that which is expected on the basis of the fireball model. Westfall *et al.*[13] estimated the temperature ($T=29$ MeV) and velocity ($\beta=0.22$) of the projectile fireball, and using these estimates we find that the width of the momentum distribution is $\sigma\sim\sqrt{m_pT}=165$ MeV/c, which is compatible with the observed value.

The projected angular distribution for He fragments is shown in Fig. 2(b). Here a single Gaussian distribution is fitted and we obtain $\sigma_1=3.11$, which corresponds to a momentum width of $\sigma(p)=140$ MeV/c. It is obvious from Table V that the observed value is compatible with the theory of Lepore and Riddle[11] and with that of Greiner *et al.*[12]

In Sec. III B, we learned that events with $Z_f\geq 6$ basically represent the peripheral-type collisions having larger impact parameters. Here, Z_f represents the charge of the projectile fragment. It was thought that we may study $\sigma(\theta)$ as a function of Z_f and estimate $\sigma(p)$ in order to see the effect of collision type on the projectile fragments. Figure 3 shows the variation of $\langle\theta_p\rangle$ vs Z_f. Here we are using the whole sample of events without being restricted to a particular type. It is seen that $\langle\theta_p\rangle$ decreases linearly with increasing Z_f for $Z_f\geq 5$, whereas $Z_f\leq 3$ shows a different trend. This may be due to the fact that collision dynamics is more or less the same for events with $Z_f\geq 5$. In Sec. III B we did observe the constancy in $\langle N_h\rangle$ for $Z_f\geq 5$, which again supports the idea that the collision characteristics are the same for such events. We calculated

$$\sigma(\theta)=(\langle\theta_p^2\rangle-\langle\theta_p\rangle^2)^{1/2}$$

for events with different values of Z_f. $\sigma(p)$ is computed using Eq. (3). Figure 4 shows the variation of $\sigma(p)$ as a function of A_f. The curve of the form

$$\sigma(p)=\sigma_0\{4f(B-f)/B^2\}^{1/2}$$

(where B and f represent, respectively, the mass numbers of the beam and fragment) is drawn though the data points calculated for $\sigma_0=182$ MeV/c. χ^2/d.f. for nine data points is equal to 0.71. Table VI compares values of σ_0 obtained by other investigators who used different techniques. Table VI also lists the theoretically predicted values for comparison. The present estimate of σ_0 is compatible with the theoretically predicted values. Furthermore, σ_0 can be related to the Fermi momentum (p_F) of

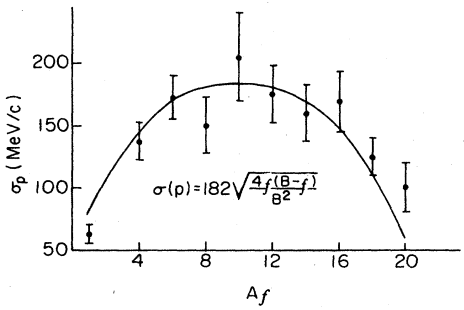

FIG. 4. The plot of momentum distribution $\sigma(p)$ in MeV/c determined from Eq. (3) versus fragment mass in atomic mass units. The curve corresponds to a fit due to the equation $\sigma(p)=\sigma_0\{[4f(B-f)/B^2]\}^{1/2}$.

TABLE VI. Comparison of the experimental and theoretical parameters related to $\sigma(p)$.

Reference	Parameter σ_0 (MeV/c)	p_F (MeV/c)	kT (MeV/nucleon)
This experiment	182	177	7.1
Lepore and Riddell (Ref. 11)	176		
Feshbach and Huang (Ref. 14)	212 for ^{16}O		
Electron scattering (Ref. 16)		230 for ^{16}O	

the projectile assuming the emission of virtual clusters according to the theory of Feshbach and Huang.[14] Using the formulation of Goldhaber,[15] the relation between $\sigma(p)$ and p_F is $p_F=B\sqrt{20\sigma_0^2(B-1)}$. The computed p_F is also listed in Table VI along with the value obtained from the electron scattering[16] experiment. It is worth mentioning that in the present investigation, projectile Fermi momentum is determined via nuclear fragmentation. If it is assumed that the projectile comes to thermal equilibrium at temperature T, the observed σ_0 can be related to T as $KT=4\sigma_0^2/m_nB$, where m_n is the nucleon mass and K is Boltzmann's constant. We see from Table VI that the excitation energy KT per nucleon is compatible with the binding energy per nucleon of the projectile, indicating

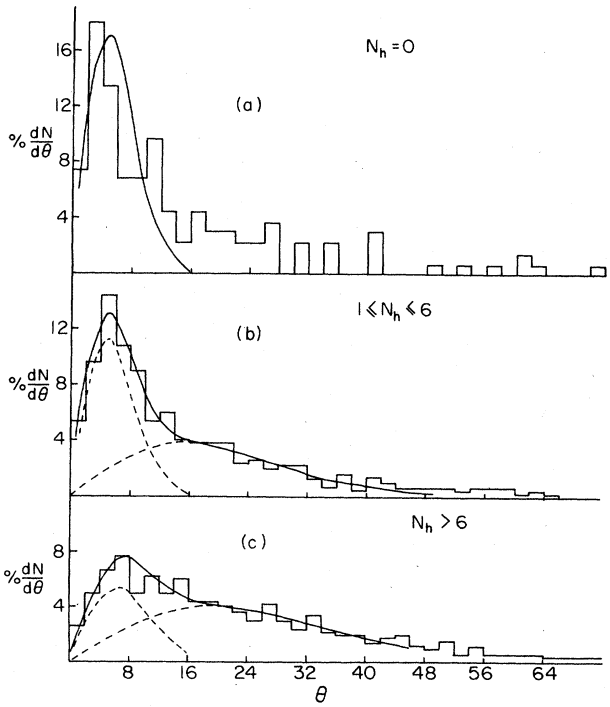

FIG. 5. Histograms representing the space angle distributions for protons for (a) $N_h=0$, (b) $1\leq N_h\leq 6$, and (c) $N_h>6$ events. The curves are the best fit due to Boltzmann distribution calculated using equation (6) of Ref. 1, dotted curves represent peak or tail regions, whereas the solid curves are for the sum.

thereby very little energy transfer between the fragment and the target. Thus we may state that the present results are compatible with those obtained from the single particle inclusive spectra. Also, we do not see any significant difference between the momentum distribution of the fragments which are produced in various kinds of interactions with different degrees of target excitation and those selected only on the basis of high rapidity without the knowledge of target excitation. This result may be regarded as a characteristic feature of limiting fragmentation. Also, we noticed that the present results at low energy are compatible with those at high energy, which again renders support to the hypothesis of limiting fragmentation.

D. Boltzmann distribution and the fireball model

In this subsection we present the results on the production of singly and doubly charged particles. It is observed that large fractions of the singly and doubly charged particles are emitted as a result of fragmentation of a projectile, whereas small fractions at large angles are emitted from a thermal source such as a fireball formed from the nucleons mutually swept out from the projectile and target.

Figure 5 shows the angular distribution of singly charged particles, which are mostly protons, as the pion production at this energy is negligible. Data have been grouped into three categories depending on the number of N_h, viz., (i) $N_h=0$, (ii) $1\le N_h\le 6$, and (iii) $N_h>6$. It is seen that these distributions have peaks along with long tails. For large N_h values, the distributions have broader peaks and much larger tails than those for small values of N_h. In order to have a quick idea of these characteristics, a parameter representing the ratio of the number of protons in a tail to a peak is calculated for each sample and is defined as

$$R_{tp}=\frac{N_t(\theta_p<\theta\le\theta_t)}{N_p(\theta<\theta_p)}\ , \tag{6}$$

where θ represents the angle of emission of the particle with respect to the beam direction; θ_p and θ_t represent, respectively, the limiting angles which a proton from the peak and from the tail can have; and N_t and N_p represent the number of protons in the tail and the peak, respectively. In the present analysis, we have taken $\theta_p=20°$ and $\theta_t=45°$. Table VII lists the R_{tp} values for different samples. It is seen that R_{tp} increases as N_h increases. Even for $N_h=0$, protons are seen at much larger angles than expected from projectile fragmentation.

An attempt has been made to fit these distributions with the moving Boltzmann distributions. $N_h=0$ events are well described by a single Boltzmann distribution, though some particles are observed at large angles. The curve drawn through the data points is obtained from the moving Boltzmann distribution. Here, the pure projectile fragmentation corresponds to a fireball with projectile velocity $\beta=\beta_p$ and a temperature of a few MeV. It is found that $T=3$ MeV describes the data reasonably well. As is obvious from Figs. 5(b) and (c), we need to have two distributions, viz., one describing the fragmentation peak representing the fireball moving with the projectile velocity and another representing the tail part which represents the fireball moving with slightly less velocity and heated to a higher temperature. Here we used exactly the same procedure as described in Ref. 1. Using the fireball formalism and the procedure for estimating β_t and T_t, we carried out the fits for different samples. The resulting

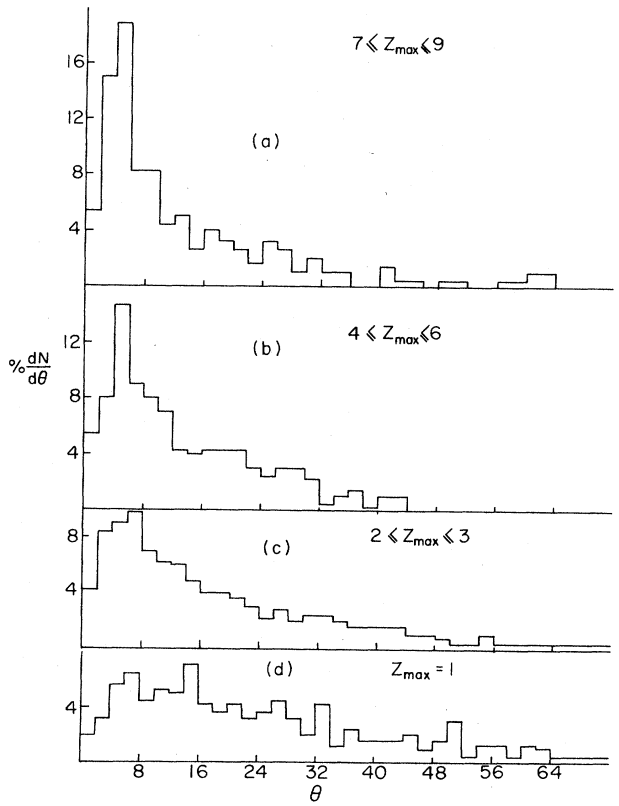

FIG. 6. The space angle distributions for protons for (a) $7\le Z_{max}\le 9$, (b) $4\le Z_{max}\le 6$, (c) $2\le Z_{max}\le 3$, and (d) $Z_{max}=1$ events.

TABLE VII. Values of different parameters for proton angular distributions for different kinds of interactions.

Sample	R_{tp}	T_t (MeV)	β_t	T_p (MeV)
$N_h=0$	0.31±0.05			3
$1\le N_h\le 6$	0.38±0.03	18.5	0.44	3
$N_h>6$	0.89±0.04	25.0	0.40	5

TABLE VIII. R_{tp} values for proton angular distributions, grouped depending on the charge of the heaviest fragment, i.e., Z_{max}.

Sample	R_{tp}
$Z_{max}=1$	1.13±0.08
$2\le Z_{max}\le 3$	0.56±0.03
$4\le Z_{max}\le 6$	0.45±0.04
$7\le Z_{max}\le 9$	0.33±0.05

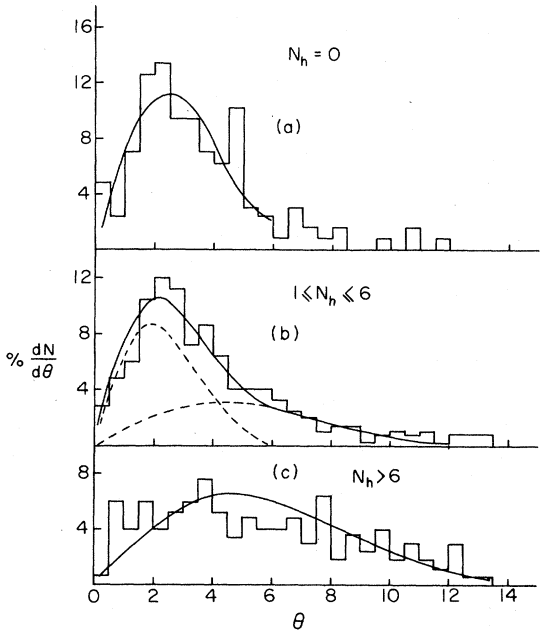

FIG. 7. Histograms representing the space angle distributions for α particles for (a) $N_h=0$, (b) $1 \leq N_h \leq 6$, and (c) $N_h > 6$ events. The curves are the best fit due to Boltzmann distribution calculated using equation (6) of Ref. 1, dotted curves represent peak or tail regions, whereas the solid curves are for the sum.

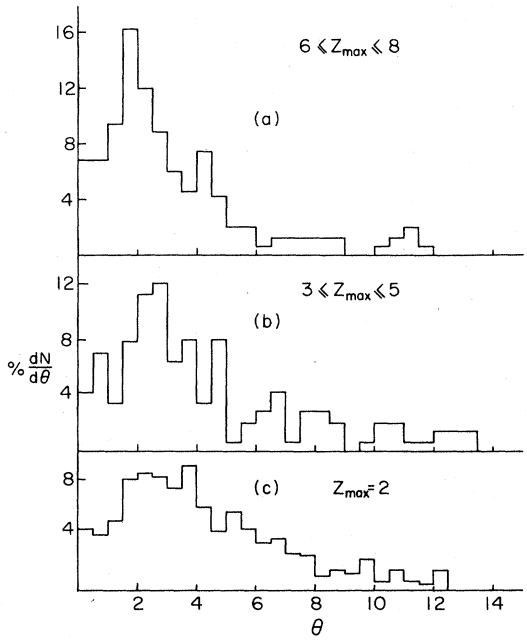

FIG. 8. The space angle distributions for α particles for (a) $6 \leq Z_{\max} \leq 8$, (b) $3 \leq Z_{\max} \leq 5$, and (c) $Z_{\max}=2$ events.

values of β_t, T_t, β_p, and T_p are listed in Table VII. From the table it is seen that the peak temperature, T_p, is greater for the $N_h > 6$ sample, which shows that the projectile is heated more than is expected from a pure projectile fragmentation process. Thus it is seen that there are two types of thermal sources: one cold, representing the peak of the distribution, and the other hot, representing the tail of the distribution.

Events have also been grouped depending on the charge of the heaviest projectile fragment $Z_{\max}$ present in an event. Figure 6 shows the angular distributions of protons for different $Z_{\max}$ groupings. Table VIII lists the R_{tp} values for different $Z_{\max}$ groupings. It is seen that distributions exhibit broader peaks and increasing tails with decreasing $Z_{\max}$. It is seen from Table VIII that R_{tp} increases as $Z_{\max}$ decreases. We may notice here that events with $Z_{\max}=1$ can be described by a single Boltzmann distribution corresponding to a fireball heated to a much higher temperature, whereas for $Z_{\max} \geq 2$, two distributions are again needed, one for the fragmentation peak and the other for a tail part. From Tables VII and VIII it is seen that R_{tp} for events with $7 \leq Z_{\max} \leq 9$ is close to that for events with $N_h=0$, and R_{tp} for events with $Z_{\max}=1$ is greater than for events with $N_h > 6$.

The angular distributions of α particles for different N_h groupings are displayed in Fig. 7. For $N_h=0$ the distribution has a broader peak with a small tail, distributions for $1 \leq N_h \leq 6$ show broader peaks and longer tails, and the distribution for $N_h > 6$ seems to have no fragmentation peak. R_{tp} values for different samples are listed in Table IX for $\theta_p=6°$ and $\theta_t=14°$. R_{tp} increases as N_h increases. The curves drawn in Fig. 7 are computed in the same way as explained in Ref. 1. It is seen that $N_h=0$ events are well described by a single moving Boltzmann distribution representing the fireball moving with the projectile velocity and having temperature $T=3$ MeV. Again, using the fireball formalism and the procedure for estimating β_t and T_t (described in Ref. 1), we carried out the fits for different samples. Table IX lists the values of different parameters for different samples. There seem to exist two thermal sources for events with $1 \leq N_h \leq 6$, one representing the fragmentation peak ($T_p=2$ MeV), the other representing the tail of the distribution formed by a fireball mechanism.[1] The distribution for events with $N_h > 6$ in Fig. 7(c) is a broad distribution without a frag-

TABLE IX. Values of different parameters for α-particle angular distributions for different kinds of interactions.

Sample	R_{tp}	T_t (MeV)	β_t	T_p (MeV)
$N_h=0$	0.13±0.04			3
$1 \leq N_h \leq 6$	0.23±0.03	8	0.51	2
$N_h > 6$	0.75±0.09	9	0.50	

TABLE X. R_{tp} values for α-particle angular distributions, grouped depending on the charge of the heaviest fragment, i.e., $Z_{\max}$.

Sample	R_{tp}
$Z_{\max}=2$	0.32±0.03
$3 \leq Z_{\max} \leq 5$	0.37±0.06
$6 \leq Z_{\max} \leq 8$	0.15±0.03

mentation peak which can be fitted to one Boltzmann distribution with $T_t = 9$ MeV and $\beta_t = 0.51$.

Figure 8 shows the angular distributions of α particles for different categories depending on the charge of the heaviest fragment emitted in an event. Table X lists the R_{tp} values for these three categories, viz., $8 \leq Z_{\max} \leq 6$, $5 \leq Z_{\max} \leq 3$, and $Z_{\max} = 2$. It is again seen that R_{tp} increases with decreasing $Z_{\max}$ as has been observed for proton angular distributions. The distribution in Fig. 8(a) for $8 \leq Z_{\max} \leq 6$ events seems to have only fragmentation peaks, as in the case of $N_h = 0$ events, whereas for distributions in Figs. 8(b) and (c), two thermal sources are needed—one representing the fragmentation peak and the other describing the tail of the distribution.

IV. CONCLUSION

The present study has revealed the following conclusions.

The observed interaction cross sections for heavy ions are comparable with those computed using a modified Eq. (2) with $r_0 = 1.36$ and $b_0 = 1.3$, rather than Eq. (1). The partial production cross sections for different kinds of fragments are identical within the statistical errors for two energies except for He and Li fragments. The partial production cross section decreases with an increasing number of He fragments. $\langle N_h \rangle$ seems to be constant for the production of one to three He fragments. It is observed that about 70% of the Li fragments are produced along with the emission of at least one more Li or together with one or more He fragments. About 65% of the O fragments are emitted along with one He fragment. It seems that modes of fragmentation are almost the same for ^{20}Ne and ^{16}O nuclei, except for small differences which are primarily due to the differences in their masses.

The two product fragmentation cross section at this energy is (36 ± 8) mb. We see that this cross section is highly suppressed with an increase in the incident energy.

$\langle N_h \rangle$ is a decreasing function of $Z_{\max}$ for $Z_{\max} < 6$, whereas for $Z_{\max} \geq 6$, it is almost constant. $\langle n_p \rangle$ decreases as $Z_{\max}$ increases. Also, $\langle \theta_p \rangle$ for $Z_f \geq 5$ decreases linearly with increasing Z_f.

We observe that the projected angular distributions of fragments are consistent with that expected from the longitudinal momentum distributions. The related parameters, e.g., Fermi momentum, excitation energy, etc., extracted from this study are consistent with the theoretically expected values.

Angular distributions of singly and doubly charged particles produced in $N_h = 0$ events are well described by a fragmentation peak, though some particles are seen at large angles. For events with $N_h > 0$, two Boltzmann distributions are needed—one representing the fragmentation peak heated to a few MeV and another representing the tail heated to much higher temperatures (~ 28 MeV). It is possible to separate the events described by one thermal source heated to about ~ 30 MeV, e.g., $N_h > 6$, for the production of α particles.

ACKNOWLEDGMENTS

We are grateful to the staff of the Bevalac at Lawrence Berkeley Laboratory, particularly to Dr. E. J. Anisworth, Dr. J. Howard, and Dr. A. Chatterjee for their help with the exposure of the emulsion stack and to Vandana Rani for her help in the data collection. This research work was supported in part by the National Science Foundation under Grant No. NSF/PHY 83-04019 and in part by Grant No. RO1-CA2487802 awarded by the National Cancer Institute, the Department of Health, Education, and Welfare.

[1] M. M. Aggarwal, K. B. Bhalla, G. Das, and P. L. Jain, Phys. Rev. C **27**, 640 (1983).
[2] C. F. Powel, P. H. Fowler, and D. H. Perkins, *The Study of Elementary Particles by the Photographic Method* (Pergamon, New York, 1959); P. L. Jain, Nuovo Cimento **13**, 839 (1959).
[3] H. C. Bradt and B. Peters, Phys. Rev. **77**, 54 (1950).
[4] W. H. Barkas, *Nuclear Research Emulsions* (Academic, New York, 1963), Vol. 1.
[5] G. D. Westfall *et al.*, Phys. Rev. C **19**, 1309 (1979).
[6] S. Barshay, C. B. Dover, and E. P. Vary, Phys. Rev. C **11**, 360 (1975); Phys. Lett **51B**, 5 (1974).
[7] R. Kullberg, K. Kristiansson, B. Lindkvist, and I. Otterlund, Nucl. Phys. **A280**, 491 (1977).
[8] B. Jakobsson and R. Kullberg, University of LUND Report No. LVIP-CR-75-14, 1975.
[9] B. Judek, in *Proceedings of the 14th International Conference on Cosmic Rays, 1975,* edited by Klaus Pinkau (Max-Planck-Institut, München, 1975), p. 2342.
[10] H. H. Heckman, D. E. Greiner, P. J. Lindstrom, and H. Shwe, Phys. Rev. C **17**, 1735 (1978).
[11] J. Y. Lepore and R. J. Riddell, Jr., Lawrence Berkeley Laboratory Report No. LBL-3086, 1974 (unpublished).
[12] D. E. Greiner *et al.*, Phys. Rev. Lett. **35**, 152 (1975).
[13] G. D. Westfall *et al.*, Phys. Rev. Lett. **37**, 1202 (1976).
[14] M. Feshbach and K. Huang, Phys. Lett. **47B**, 300 (1973).
[15] A. S. Goldhaber, Phys. Lett. **53B**, 306 (1974).
[16] E. J. Moniz *et al.*, Phys. Rev. Lett. **26**, 445 (1971).